Journal of Alloys and Compounds 509 (2011) 636–643

Contents lists available at ScienceDirect

Journal of Alloys and Compounds

journal homepage: www.elsevier.com/locate/jallcom

Influence of the thermal treatment on the deformation-induced precipitation of a hypoeutectic Al–7 wt% Si casting alloy deformed by high-pressure torsion

C.M. Cepeda-Jiménez[a,*], J.M. García-Infanta[a], A.P. Zhilyaev[a,b], O.A. Ruano[a], F. Carreño[a]

[a] Department of Physical Metallurgy, CENIM, CSIC, Av. Gregorio del Amo 8, 28040 Madrid, Spain
[b] Institute for Metals Superplasticity Problems, Russian Academy of Science, 39 Khalturina, 450001 Ufa, Russia

ARTICLE INFO

Article history:
Received 10 August 2010
Received in revised form
21 September 2010
Accepted 22 September 2010
Available online 1 October 2010

Keywords:
Al–Si alloys
High-pressure torsion
Deformation-induced precipitation
Microstructure
Mechanical properties

ABSTRACT

A hypoeutectic Al–7 wt% Si alloy was subjected to high-pressure torsion (HPT) at room temperature using an imposed pressure of 6 GPa and torsional straining through five revolutions. Different thermal treatments, prior to the HPT processing, resulted in reducing supersaturated Si concentration in comparison to the as-cast material. Microstructural parameters and microhardness were evaluated in the present work. Processing by HPT produced significant grain refinement with grain sizes of about 200–400 nm. Furthermore, fine deformation-induced Si precipitates from the supersaturated solid solution were observed, which are very useful in retaining the fine microstructure during HPT processing. The microhardness increase was outstanding, with values for processed samples twice higher (84 HV) than that for the as-cast Al–7 wt% Si alloy (44 HV). The results demonstrate that the refining and strengthening of the Al matrix by HPT processing depend on the available supersaturated solid solution during the processing.

1. Introduction

Al–Si eutectic alloys are widely used in industry, especially in the automobile industry, due to their good wear resistance, high tensile strength at elevated temperatures and good castability [1–4]. However, its low fracture toughness impedes broader applications of these alloys. The low fracture toughness originates in the microstructure, which consists of eutectic silicon second phase in an aluminium alloy matrix. Application of severe plastic deformation for processing of Al–Si alloys has been performed showing how breaking up this microstructure and dispersing the eutectic silicon results in improved impact toughness, strength, ductility and wear resistance [1,5–8].

Several procedures are available for imposing severe plastic deformation but one of the most attractive techniques, currently receiving maximum attention, is high-pressure torsion (HPT). HPT creates intense strain in materials, thus producing an ultrafine-grained structure and helping to modify the distribution of second phase particles, which are usually sheared during deformation [9–11].

Experiments have shown that the ultrafine-grained structures developed during severe plastic deformation are reasonably stable at elevated temperatures when the matrix alloy contains a fairly uniform dispersion of precipitates [12].

It is well known that in aluminium-based alloys the introduction of second-phase particles to pin grain boundary migration [13,14], or the use of solute to inhibit recovery [15,16], are effective approaches for decreasing the grain size. Accordingly, the effectiveness of the severe plastic deformation on microstructure evolution will depend on the initial solute content [17], and the size and distribution of second phases [13,18]. Additionally, dynamic processes such as solute precipitation [19–21] or dissolution [22] may occur during large strain deformation and influence the extent and nature of microstructure refinement.

Recently, it was found that different concentrations of solid solution in Al–7 wt% Si alloy produced different grain sizes and mechanical properties in this material processed by ECAP [21].

Therefore, the aim of this work was to examine microstructure refinement in the aluminium matrix of an Al–7 wt% Si processed by HPT, considering the influence of the initial Si concentration in supersaturated solid solution, as well as the role of second-phase particles. Microstructure evolution is followed by measuring grain size and also examining the size distribution of eutectic silicon particles present in the highly strained materials. Mechanical behaviour is examined by Vickers microhardness testing.

2. Experimental procedure

Pure Al (99.99 wt%) and Al–12.3 wt% Si–0.02 wt% Na alloy were melted and casted into a mould to produce an ingot having dimensions of 400 mm × 250 mm × 40 mm. Emission spectroscopy of the resulting material revealed a composition (in wt%) of 7.0% Si, 0.3% Fe and balance Al. Disk samples

* Corresponding author. Tel.: +34 91 5538900x217; fax: +34 91 5347425.
E-mail address: cm.cepeda@cenim.csic.es (C.M. Cepeda-Jiménez).

0925-8388/$ – see front matter © 2010 Elsevier B.V. All rights reserved.
doi:10.1016/j.jallcom.2010.09.122

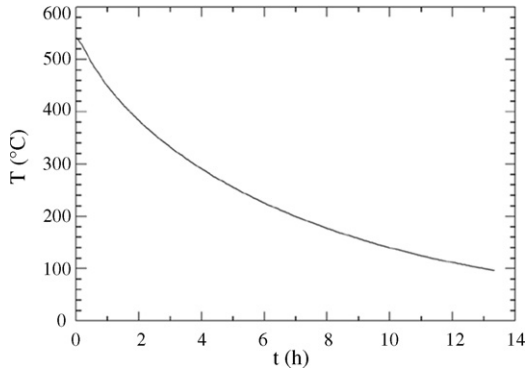

Fig. 1. Temperature vs. time during slow cooling inside furnace of the S sample.

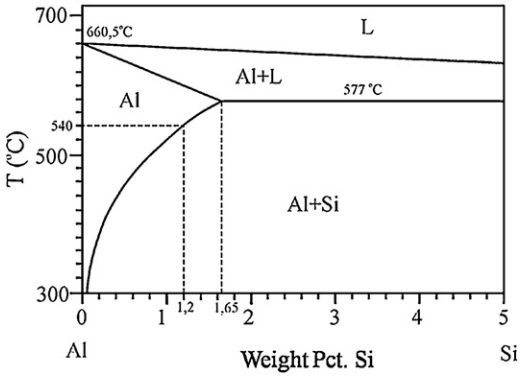

Fig. 2. Detail of the Al–Si phase diagram from 0 to 5 wt% Si.

for HPT were machined with dimensions ~0.85 mm thick and 10 mm in diameter. Samples processed in the as-cast condition are referred to here as C samples. Additional samples were subjected to two different heat treatment sequences prior to HPT processing to control and reduce the supersaturated Si concentration in the as-cast material: (a) annealing at 540 °C for 20 h, followed by water quenching to room temperature (referred to here as Q samples), and (b) annealing at 540 °C for 20 h followed by slow cooling inside the furnace over 13.5 h (referred to here as S samples). The temperature during cooling of the S samples was recorded and is shown in Fig. 1.

The three sets of samples were then subjected to HPT processing at room temperature through five whole revolutions using a constrained HPT facility [23,24], under an applied load of 6 GPa. Details on the principles of HPT were given earlier [25]. The final thickness of the HPT samples was ~0.65 mm.

HPT processed samples were characterized using both optical and scanning electron microscopy, and microhardness measurements.

Metallographic observation involved methods of standard surface preparation. The samples were mechanically polished and then electropolished in a 30% nitric acid solution in methanol at −28 °C and 17 V. Microstructure both in the central regions of the disks and near the edges was observed by scanning electron microscopy (SEM), using a JEOL JSM 6500F equipment with field emission gun. EDX analysis to identify the concentration of silicon within the aluminium dendrites was performed by an electron probe microanalyzer (Oxford Inca) operating at 15 kV.

Grain size was measured on the primary Al constituent for all the processed conditions from SEM images obtained using backscattered electrons. Eutectic Si particle sizes were measured by optical microscopy. Optical and scanning electron micrographs were analyzed using the Sigma Scan Pro software in order to obtain the size distribution of the Si precipitates and aluminium matrix grains. Due to the particles not being spherical in the alloy, the maximum dimension of the particle was used as the particle size. More than 550 precipitates and 200 grains for each thermal condition were analyzed. Size distribution histograms obtained from these measurements were conducted. Particles and grain size data fell into log-normal distributions, so the geometric mean value was chosen as a measure of their size.

Vickers microhardness was measured along diameters of HPT disks using a Matsuzawa Seiki MHT-1 microhardness tester, using a load of 1 kg for 15 s for the unprocessed samples, and 100 and 200 g for 15 s for the HPTed materials. The distance from each indentation to the centre of the disk was measured from the indentation centre using the Sigma Scan Pro image analysis software.

3. Results

3.1. Materials

Fig. 2 shows the phase diagram of the Al–Si system [26]. The eutectic is formed between an aluminium solid solution containing only 1.65 wt% silicon (at the eutectic temperature, 577 °C), and virtually pure silicon as the second phase. EDX measurements (Table 1) reveal that following solidification, i.e. for the as-cast material referenced as C sample, 1.6 wt% Si is retained in supersaturated solid solution within the middle of primary Al dendritic cells. The Si solid solution amount was quantified in the middle of the Al dendrites to discard the contribution from eutectic Si particles. Additionally, in this study, annealing at 540 °C for 20 h followed either by quenching (Q sample) or slow cooling (S sample) has been employed to control and reduce this supersaturated Si concentration. According to the phase diagram (Fig. 2), Si solubility at 540 °C amounts 1.2 wt%, which means that 0.5 wt% of Si has already segregated to the eutectic constituent. The EDX measurements confirm 1.1 ± 0.2 wt% Si for the annealed and quenched Q sample and 0.7 ± 0.1 wt% Si for the furnace cooled S sample.

3.2. Microstructure

Fig. 3 shows optical micrographs at two magnifications of the Si particle distribution in the as-cast alloy (C sample), and after thermal treatments to modify the solid solution in the Al matrix (Q and S samples). The microstructure of the Na-modified Al–7 wt% Si in the as-cast condition (Fig. 3a and b) consists of large grains, including the primary Al dendrites, which are surrounded by the interdendritic network of eutectic constituent, which contains a distribution of mainly irregular Si fibres, and a small volume fraction of needle-like Al_5FeSi phase consequence of Fe impurities on the alloy.

After annealing at 540 °C for 20 h (Fig. 3c–f), coarsening and slight spheroidization of the silicon particles occurs. In addition, disappearance of small Si particles inside the eutectic region is observed comparing with Fig. 3a and b.

Fig. 4 shows optical micrographs of the Si particles produced after HPT processing for samples C (Fig. 4a and b) and Q (Fig. 4c and d), at the periphery of the HPT disks. HPT processing changes the as-cast structure into a homogenous Si particle distribution in the Al matrix approximately 1 mm from the disk centre. A dendrite structure is not observed in the processed alloy.

It is apparent from a comparison of Figs. 4a and b and 3b that the rod-shaped particles visible in the as-cast C sample are no longer present, and they have been replaced by more equiaxed particles. It has been reported [27,28] that large and long particles are very prone to cracking during severe plastic deformation due to the fact that the load transfer process for this morphology is very efficient. Thus, it is our contention that the Si and Al_5FeSi particles were broken during processing and became more equiaxed in morphology. Moreover, the average particle size clearly has increased for the HPTed C sample. This indicates that there is initial fragmentation of the three dimensional network of silicon fibres during

Table 1
Silicon concentration (wt%) in the middle of aluminium dendritic cells for Al–7 wt% Si alloy samples, as a function of different thermal treatments.

Sample	Si (wt%)
As-cast (C)	1.6 ± 0.2
540 °C-20 h + quenching (Q)	1.1 ± 0.2
540 °C-20 h + slow cooling (S)	0.7 ± 0.1

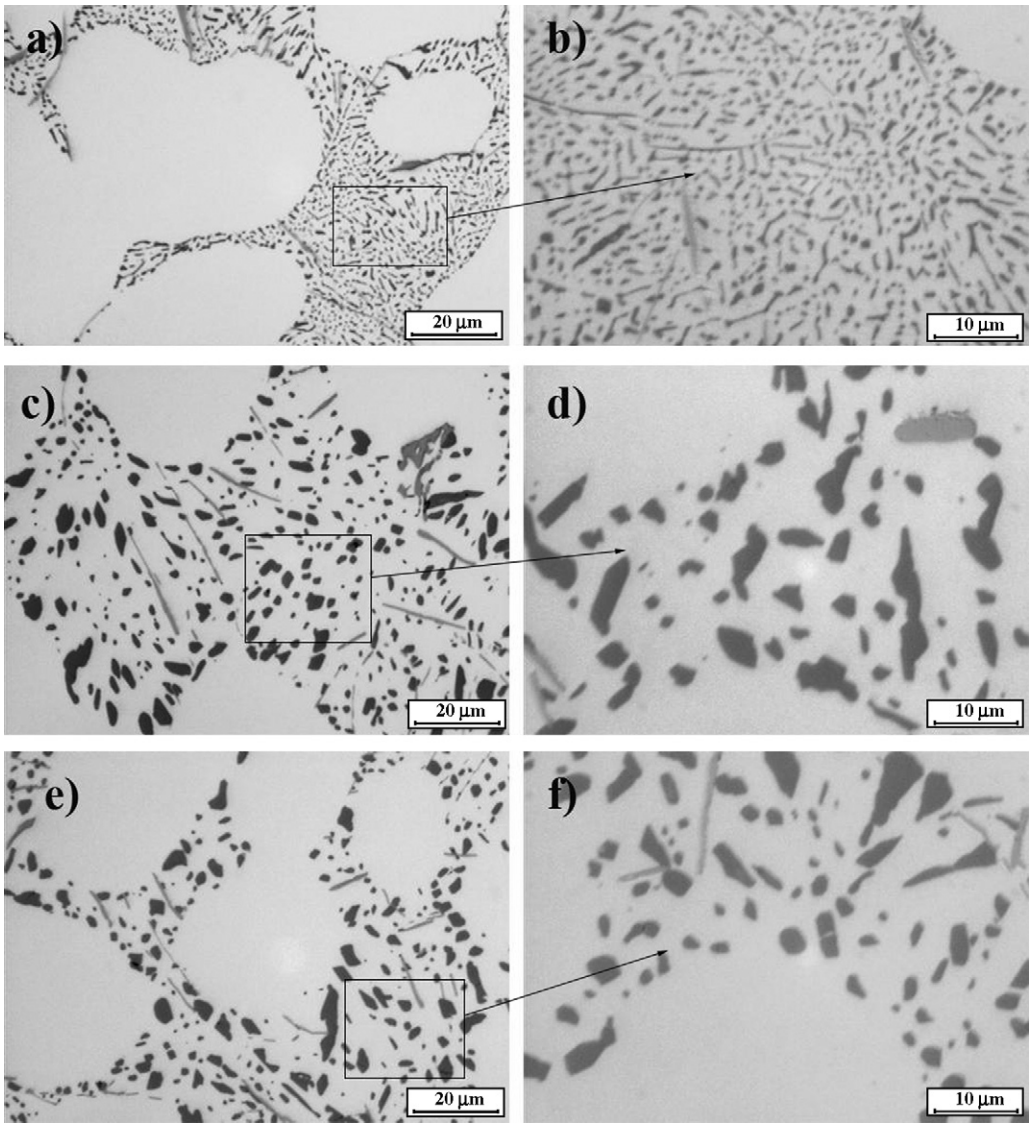

Fig. 3. Optical micrographs at two magnifications of the eutectic Si particles in the Al–7 wt% Si alloy subjected to different thermal treatments: (a) and (b) as-cast C sample; (c) and (d) annealed and quenched Q sample; (e) and (f) annealed and furnace cooled S sample.

processing, followed by additional coarsening in subsequent torsion straining. Additionally, for the processed Q sample (Fig. 4c and d) the Si particle morphology changed slightly in comparison with the un-processed sample (Fig. 3c and d). It is important to note from inspection of the micrographs, that the silicon particle size and spacing in the HPTed C sample are smaller than those for the annealed samples.

Fig. 5 illustrates the particle size distribution in the different Al–7 wt% Si samples after HPT processing. For the HPTed-C sample over 55% of the silicon particles are smaller than 2.5 μm, while for the processed Q and S samples only 20% of the silicon particles are smaller than this value. Additionally, the size distribution histogram for C sample is sharper with less data dispersion than that for the annealed and processed samples. These results indicate that the annealing treatment prior to the HPT processing has important influence on the final size and distribution of large silicon particles after straining.

Matrix grain microstructure for the processed C sample at the periphery of the HPT disks is illustrated in Fig. 6 by secondary electron micrographs (Fig. 6a), and crystallographic contrast using backscattered electrons (Fig. 6b and c). No visible difference in the Al matrix microstructure between the centre and the periphery of the HPT samples was found.

It is immediately apparent from Fig. 6b that the grain size is refined, and furthermore, two zones, delineated by a broken line, with different grain sizes are clearly observed. In addition, by secondary electron image (Fig. 6a), the precipitation of small Si particles (<100 nm in size) within the aluminium matrix can be observed. Inspection of the primary Al dendrite cells at high magnification, using both SE and BSE modes in the FEG–SEM for the as-cast (C sample), and thermal treated (Q and S samples) prior to HPT processing was conducted. Small precipitates in the Al matrix were not detected.

For the HPTed C sample there was evidence for small precipitates-free zones near a high fraction of the large Si particles. A larger grain size in the aluminium matrix within these zones was observed. The grain/subgrain sizes were measured from BSE images using the mean linear intercept method. Fig. 6d shows the grain size distribution histogram for the HPTed C sample taken at the ultrafine grain region. Grain size measurement gave values of ~200 nm at the zone containing small Si precipitates (Fig. 6c), and ~0.5 μm at the zone of larger grain size. In a prior work about ECAP deforma-

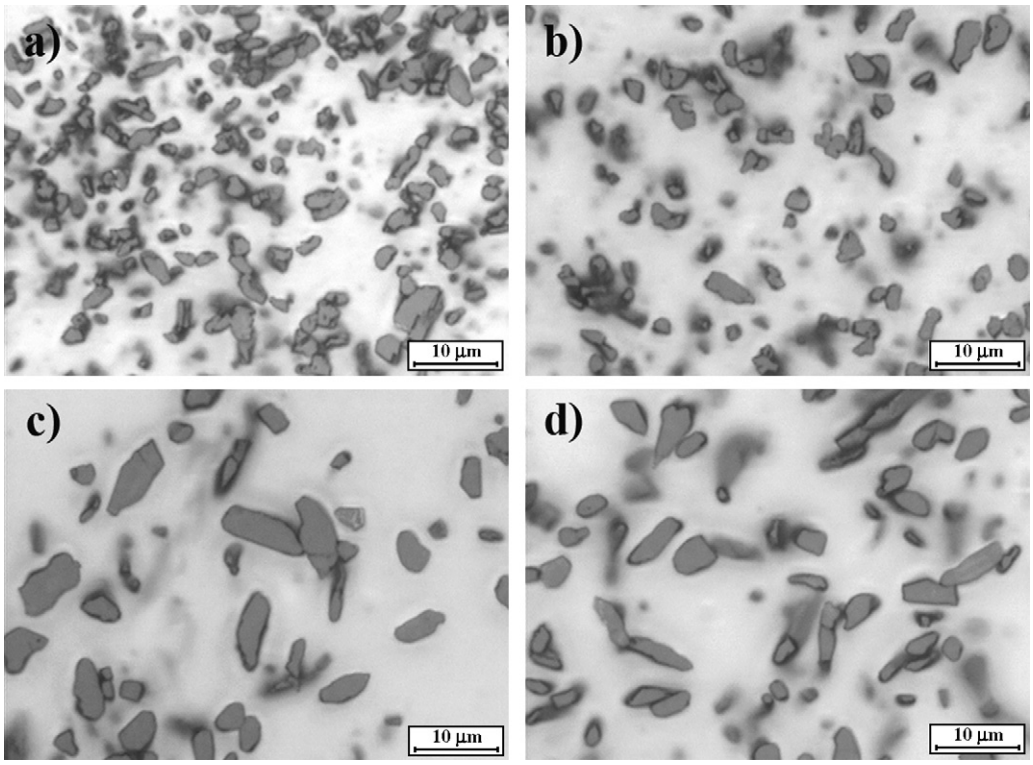

Fig. 4. Optical micrographs of the HPT Al–7 wt% Si samples showing the silicon particles: (a) and (b) C samples; (c) and (d) Q samples.

tion of Al–7 wt% Si alloy [21], an explanation for these differences in grain size was given. Fine grains evolve by processes of grain subdivision in the primary aluminium, and these grains are stabilized by deformation-induced precipitation of fine Si precipitates on the boundaries. Additionally, the absence of these small precipitates in the as-cast unprocessed samples corroborates that precipitation is induced by deformation, and takes place during the severe plastic deformation or immediately after the processing [20,21].

Fig. 7 shows secondary and backscattered electron micrographs for the HPTed S (Fig. 7a and b) and Q (Fig. 7c and d) samples, where a clear difference between the microstructures for both samples is observed. A comparison of the SE micrographs at the same magnification in Fig. 7a and c reveals higher number of nanometric Si precipitates induced by deformation in the HPTed Q sample (Fig. 7c) than in the S sample (Fig. 7a). Additionally, the corresponding BSE micrographs in Fig. 7b and d for processed S and Q samples, respectively, reveal the presence of an array of fine grains. The microstructure is visibly smaller for the Q sample, with an average grain size of ~200 nm (see grain size distribution histogram in Fig. 7f), than for the S sample with an average grain size of ~400 nm (Fig. 7e).

On the other hand, the grain size for the processed Q sample of ~200 nm is similar to that for the HPTed C sample in the UFG region, showing similar shape of the grain size distribution histograms (Figs. 6d and 7f).

Fig. 8 includes BSE micrographs, showing the grain microstructure of aluminium matrix surrounding coarse Si particles. Fig. 8a and b correspond to processed C sample, Fig. 8c to HPTed S sample and finally Fig. 8d to HPTed Q sample. In general, the microstructure for S and Q samples is essentially equiaxed and there is no evidence for the presence of any region with a coarsened structure, even close to the large eutectic Si particles. However, the microstructure corresponding to the HPTed C samples (Fig. 8a and b) shows (Fig. 6b) coarsened grains of heterogeneous size, close to the large eutectic Si particles. Thus, the microstructure in the HPTed C sample is not as homogeneous as for the thermal treated HPT processed samples (Q and S).

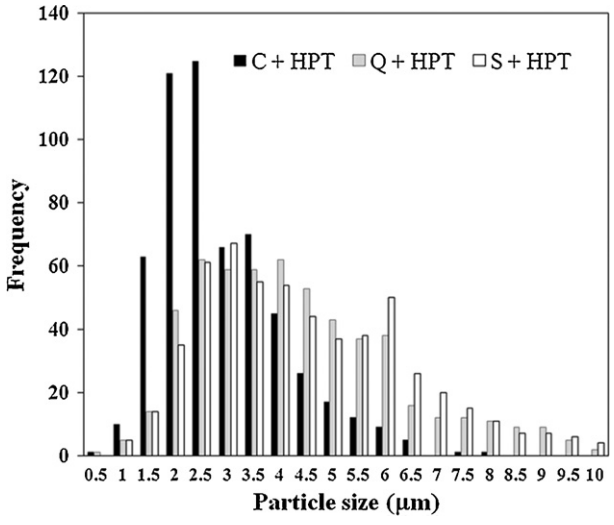

Fig. 5. Si particle size distribution histogram determined by measuring 570 particles in each HPT processed sample.

3.3. Microhardness test

Vickers microhardness is plotted in Fig. 9 as a function of distance through the diameter for the HPT samples. Values for the as-cast Al–7 wt% Si samples subjected to different thermal treatments are included for comparison. Large indentation imprints with 1 kg load were carried out to measure the contribution of the aluminium matrix and the eutectic Si particles in the un-processed

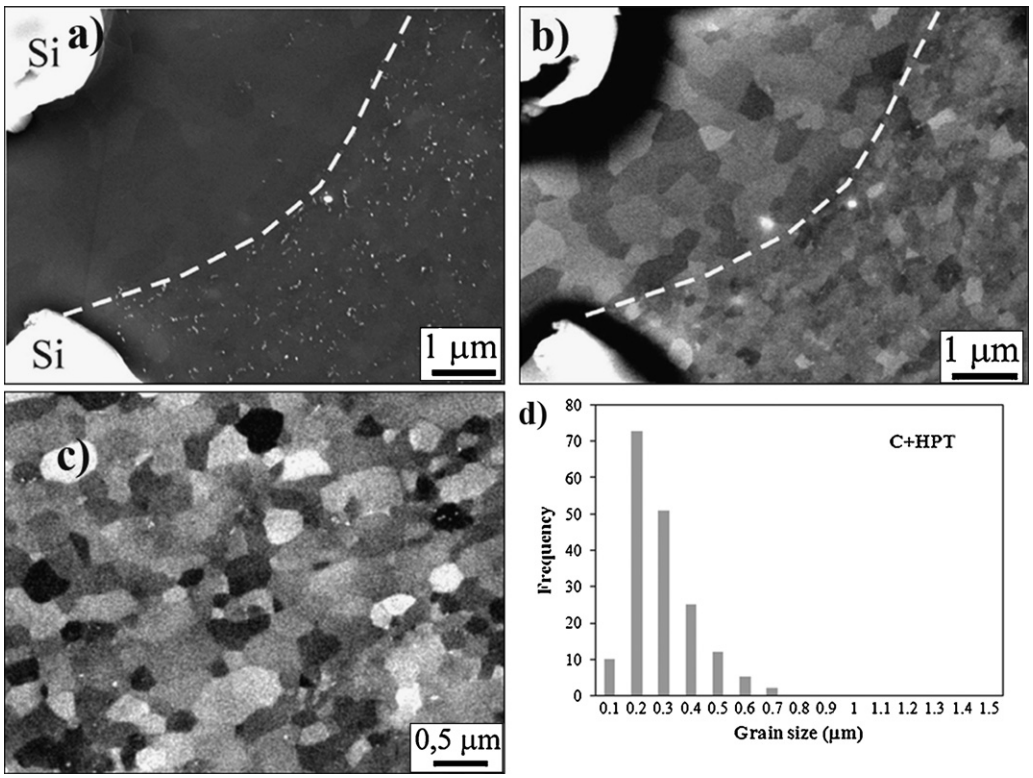

Fig. 6. (a) and (b) Secondary (SE) and backscattered (BE) electron micrographs respectively of the area around large Si particles in HPTed C sample, showing a zone with deformation-induced precipitates, and a precipitate-free zone [20]. (c) BE micrograph in the area with UFG and Si precipitates at higher magnification. (d) Grain size distribution histogram in the UFG region.

samples. On the other hand, smaller imprints using 100 and 200 g for 15 s were performed in the HPT processed materials to characterize the fine microstructure. Similar results were obtained with both indentation loads.

The lower dotted lines correspond to the un-processed samples. The microhardness value for the sample in the undeformed initial state is slightly higher for the C sample (44 HV), followed by the value for the Q sample (42 HV), and finally S sample (32 HV). The microhardness decrease after thermal treatment at 540 °C for 20 h is caused by relaxation of residual stresses and loss of solute content defined by the phase diagram (Fig. 2), which effectively reduces the number of obstacles available to impede the dislocation movement and thus, promoting an inherent softening of the material.

The hardness increase is prominent for the processed samples by HPT, and it remains constant across the diameter of the disk. The trend of the constant hardness with the distance suggests that there was a gradual development into a reasonably homogeneous microstructure [29]. The material annealed and quenched followed by HPT processing (Q sample) exhibited the highest hardness after HPT processing (84 HV), which was about twice that of the unprocessed control sample. The microhardness value (77 HV) of the as-cast HPTed material (C sample) was found, a priori unexpectedly, to lie between that of the processed Q sample and S sample (64 HV). Therefore, in consistence with the microstructures observed for HPTed samples in the present study, the processed Q sample with finest and most homogeneous microstructure shows higher average microhardness value (84 HV), than that for the C sample (77 HV), with heterogeneous distribution of both grain size and deformation-induced precipitation of small Si precipitates. Finally, the HPTed S sample shows the lowest average microhardness value (64 HV), according to its lower initial concentration of Si in solid solution, which produces fewer deformation-induced precipitates and as a result, coarser grain microstructure.

4. Discussion

The strengthening achieved by HPT processing of Al–7 wt% Si alloy is analyzed in terms of grain refinement and deformation-induced precipitation. Annealing at 540 °C for 20 h prior to HPT processing was performed to control and reduce the supersaturated Si concentration in the as-cast material for studying its influence on the processing effectiveness. After this thermal treatment, the initial content of supersaturated Si solid solution in the primary Al of the as-cast material (C samples) decreases from ~1.6 wt% to ~1.1 wt% Si for the annealed and quenched Q sample, and to ~0.7 wt% Si for the annealed and slow cooled S sample (Table 1).

After severe plastic deformation by HPT, the decrease in grain size was very noticeable in all samples considered, being this decrease smaller for the S sample (~400 nm), containing the lowest initial Si solute concentration, than that for Q and C sample with grain size of ~200 nm (Figs. 6 and 7). However, whereas the annealed and processed Q and S sample with lower initial solid solution content showed uniform grain size (Fig. 8), the HPTed C sample with the highest initial Si solid solution showed a bimodal microstructure. This microstructure consisted in UFG regions (~200 nm) where deformation-induced precipitation of fine Si particles was clearly observed (Fig. 6), and zones with coarsened grains (~0.5 μm) adjacent to the large eutectic Si particles, where deformation-induced precipitates were not present.

It is our contention that the main factor to explain the heterogeneous microstructure observed for the HPTed C sample with respect to the annealed samples, which leads to lower strengthening that expected, is the non-equilibrium state of the as-cast C sample due to the fast solidification during the casting process. The high and heterogeneous solid solution supersaturation after the

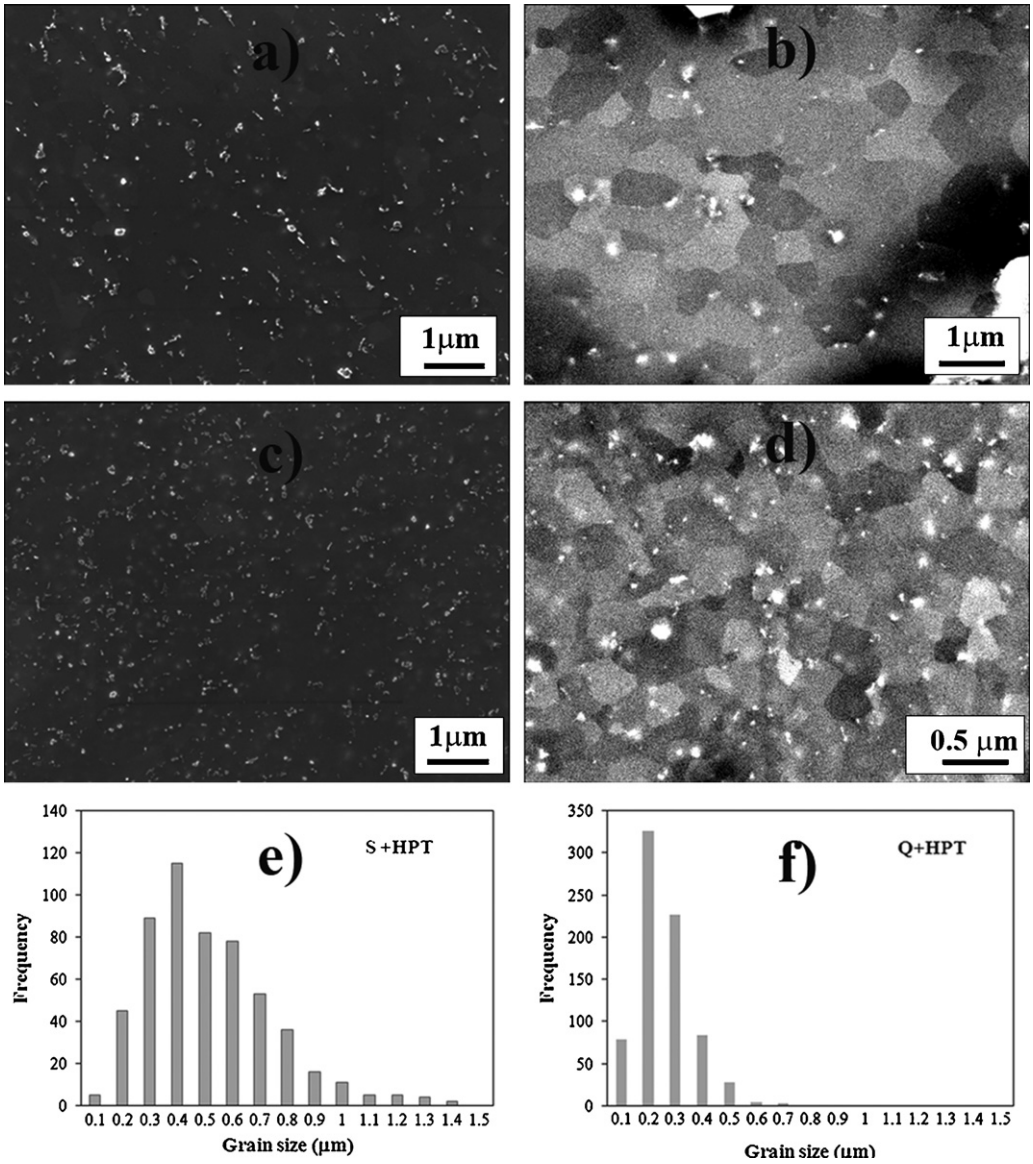

Fig. 7. (a) and (c) Secondary and (b) and (d) backscattered electron micrographs at different magnifications of the microstructure of HPTed Al–7 wt% Si samples: (a) and (b) S sample; (c) and (d) Q sample. (e) and (f) grain size distribution histograms for S and Q samples respectively processed by HPT.

cast processing increases the chemical driving force for the bulk diffusion of Si from the solid solution to the eutectic Si particles, creating areas around these particles depleted in solid solution. As consequence of this heterogeneity in solid solution concentration, less deformation-induced precipitation of fine precipitates occurs in certain zones, leading to coarsened grain areas. Therefore, the deformation-induced precipitation arising from the available local solid solution concentration for each sample will determine the grain size obtained.

On the other hand, the prolonged annealing at 540 °C for 20 h prior to HPT processing, to control the supersaturated Si content, leads to an equilibrium state, accordingly to the phase diagram (Fig. 2), decreasing the concentration gradient and thus the driving chemical force for Si diffusion [30]. As shown in Fig. 3, the eutectic Si particles were considerably coarsened by the annealing treatment of the Q and S samples, reaching a quasi-equilibrium state, since their size and morphology were scarcely modified during the following HPT processing. This indicates that substantial additional Si diffusion during HPT processing is not produced. However, it was clearly observed for the HPT processed C sample that the eutectic Si and Al_5FeSi particles were broken during processing, and coarsened considerably due to accelerated diffusion from the supersaturated solid solution assisted by the non-equilibrium state.

Additionally, it is suggested that together with the highest supersaturated solid solution and chemical driving force for the C sample, severe plastic deformation by HPT processing produces high dislocation density, especially near large eutectic Si particles, due to large local strain gradients [18]. The Si diffusion assisted by dislocations and increased chemical driving force produced consequently higher growth of the eutectic Si particles in the HPTed C sample. Moreover, as dislocations are paths for solute diffusion, the grain size increases close to the large Si particles by dynamic recovery, decreasing the pinning effect. The effect of supplying solute by dislocations to the eutectic Si particles diminishes as recovery occurs [31]. Therefore, ultrafine grains were still observed in zones where Si solid solution was enough to induce precipitation of fine Si particles, thus obtaining the bimodal microstructure previously mentioned.

Vickers microhardness results (Fig. 9) showed that whilst HPT processing increased hardness in all samples considered, the mag-

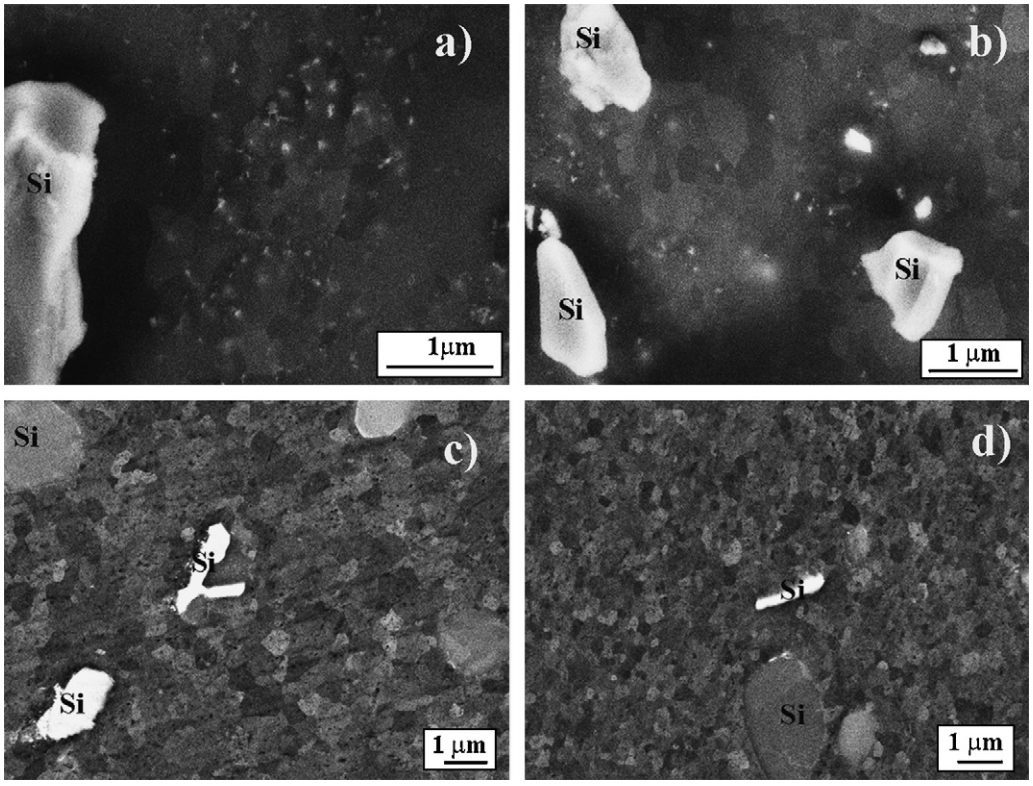

Fig. 8. BE micrographs showing the microstructure around large Si particles in HPT processed samples: (a) and (b) C samples; (c) S sample and (d) Q sample.

nitude of this increase is strongly influenced by the final grain size, which is determined by deformation-induced precipitation from the available supersaturated Si solid solution concentration. Prior to HPT, as-cast Al–7 wt% Si alloy and thermal treated samples have low hardness (~34–44 HV), and the slight differences between the samples are predominantly due to solid solution strengthening, accordingly to the estimated trend. After HPT processing, the microstructural differences between C, Q and S processed samples are reflected in the hardness of the different samples. The new size and distribution of the large eutectic Si particles after HPT does not become important for significant hardening, because they remain coarse and widely separated.

HPT processing on the sample with the lowest initial Si solid solution concentration (S) leads to larger grain size than that for the more supersaturated ones (C and Q), following the expected trend, and suggesting the important role of solute in enhancing HPT refining and strengthening by deformation-induced precipitation. On the other hand, the HPTed Q sample has shown the highest hardening, due to the finest and homogenous microstructure across the processed sample. On the contrary, HPTed C sample, initially containing the highest concentration of solid solution, showed less hardening than that for Q sample. This a priori unexpected result is thought to arise from a combination of hardening by UFG refining and deformation-induced precipitation, and softening due to loss of solute content close to the large Si particles and recovery of the deformation structure.

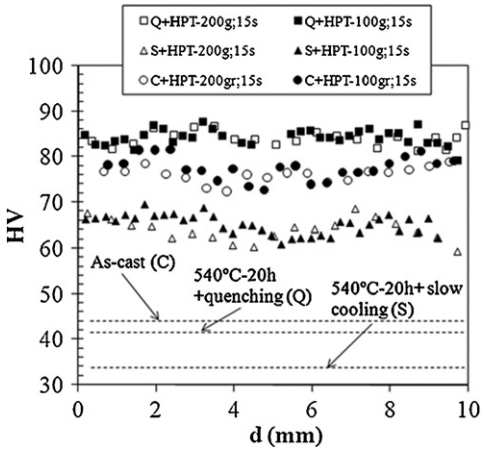

Fig. 9. Vickers microhardness vs. distance through the diameter of the HPT processed samples.

In summary, the results shown in the present study indicate that small variations in solute content and its distribution in a hypoeutectic Al–7 wt% Si alloy, as a consequence of different initial states, can lead to significant changes in microstructure and microhardness after HPT processing.

5. Conclusions

Three different samples of Al–7 wt% Si subjected to thermal treatments to control the supersaturated Si concentration were processed by HPT processing. The main conclusions of this study are as follows:

1. Severe plastic deformation by HPT of an Al–7 wt% Si alloy leads to grain refinement (~200–400 nm), which depends on the available concentration of supersaturated Si solid solution during the processing.
2. Severe deformation produces precipitation of fine particles of silicon. Such fine deformation-induced Si precipitates are very useful in retaining fine microstructures during HPT processing.
3. The microstructure was inhomogeneous for the HPTed as-cast "C" sample, having the highest Si solid solution content, due to non-equilibrium state by the casting processing and high chemical driving force. This non-equilibrium state favours diffusion

of silicon solute to large silicon particles during HPT leading to precipitate-free zones and local grain growth around these large particles. Accordingly, the measured grain size varies from very small values (~200 nm) far from the eutectic Si particles, to significantly larger values (~0.5 μm) in the vicinities of these large particles, leading to unexpected low microhardness value (77 HV).

4. The highest strengthening (84 HV) has been obtained for the annealed and quenched HPTed Q sample due to the greater degree of microstructural homogeneity, both in deformation-induced Si precipitation and grain size (~200 nm).

Acknowledgements

Financial support from MICINN (Project MAT2009-14452) is gratefully acknowledged. C.M. Cepeda-Jiménez thanks the Spanish National Research Council (CSIC) for a I3P contract, and A.P. Zhilyaev to the Spanish Ministry of Education and Science for a Ramón y Cajal contract.

References

[1] J.M. García-Infanta, A.P. Zhilyaev, C.M. Cepeda-Jiménez, O.A. Ruano, F. Carreño, Scr. Mater. 58 (2008) 138–141.
[2] A. Ma, K. Suzuki, Y. Nishida, N. Saito, I. Shigematsu, M. Takagi, H. Iwata, A. Watazu, T. Imura, Acta Mater. 53 (2005) 211–220.
[3] P. Cavaliere, E. Cerri, P. Leo, Mater. Charact. 55 (2005) 35–42.
[4] F.C. Robles-Hernández, J.H. Sokolowski, J. Alloys Compd. 480 (2009) 416–421.
[5] Y. Nishida, H. Arima, J.C. Kim, T. Ando, Scr. Mater. 45 (2001) 261–266.
[6] A. Ma, N. Saito, M. Takagi, Y. Nishida, H. Iwata, K. Suzuki, I. Shigematsu, A. Watazu, Mater. Sci. Eng. A 395 (2005) 70–76.
[7] A. Ma, K. Suzuki, N. Saito, Y. Nishida, M. Takagi, I. Shigematsu, H. Iwata, Mater. Sci. Eng. A 399 (2005) 181–189.
[8] Z.Y. Ma, S.R. Sharma, R.S. Mishra, Scr. Mater. 54 (2006) 1623–1626.
[9] R.Z. Valiev, R.K. Islamgaliev, I.V. Alexandrov, Prog. Mater. Sci. 45 (2000) 103–189.
[10] T. Tokunaga, K. Kaneko, Z. Horita, Mater. Sci. Eng. A 490 (2008) 300–304.
[11] N. Van Steenberge, S. Hóbor, S. Suriñach, A.P. Zhilyaev, F. Houdellier, F. Mompiou, M.D. Baró, Á. Révész, J. Sort, J. Alloys Compd. 500 (2010) 61–67.
[12] P.B. Berbon, N.K. Tsenev, R.Z. Valiev, M. Furukawa, Z. Horita, M. Nemoto, T.G. Langdon, Metall. Mater. Trans. A 29 (1998) 2237–2243.
[13] P.J. Apps, M. Berta, P.B. Prangnell, Acta Mater. 53 (2005) 499–511.
[14] Y.-L. Deng, L. Wan, Y. Zhang, X.-M. Zhang, J. Alloys Compd. 498 (2010) 88–94.
[15] Y. Iwahashi, Z. Horita, M. Nemoto, T.G. Langdon, Metall. Mater. Trans. A 29 (1998) 2503–2510.
[16] Y.H. Zhao, Y.T. Zhu, X.Z. Liao, Z. Horita, T.G. Langdon, Mater. Sci. Eng. A 463 (2007) 22–26.
[17] M. Furukawa, Z. Horita, M. Nemoto, R.Z. Valiev, T.G. Langdon, Acta Mater. 44 (1999) 4619–4629.
[18] P.J. Apps, J.R. Bowen, P.B. Prangnell, Acta Mater. 51 (2003) 2811–2822.
[19] H.W. Kim, S.B. Kang, N. Tsuji, Y. Minamino, Acta Mater. 53 (2005) 1737–1749.
[20] A.P. Zhilyaev, J.M. García-Infanta, F. Carreño, T.G. Langdon, O.A. Ruano, Scr. Mater. 57 (2007) 763–765.
[21] J.M. García-Infanta, S. Swaminathan, C.M. Cepeda-Jiménez, T.R. McNelley, O.A. Ruano, F. Carreño, J. Alloys Compd. 478 (2009) 139–143.
[22] A. Korchef, Y. Champion, N. Njah, J. Alloys Compd. 427 (2007) 176–182.
[23] A.P. Zhilyaev, S. Lee, G.V. Nurislamova, R.Z. Valiev, T.G. Langdon, Scr. Mater. 44 (2001) 2753–2758.
[24] A.P. Zhilyaev, K. Oh-ishi, T.G. Langdon, T.R. McNelley, Mater. Sci. Eng. A 410–411 (2005) 277–280.
[25] A.P. Zhilyaev, B.K. Kim, J.A. Szpunar, M.D. Baró, T.G. Langdon, Mater. Sci. Eng. A 391 (2005) 377–389.
[26] J.L. Murray, A.J. MacAlister, Bull. Alloy Phase Diagr. 5 (1984) 74–84.
[27] C.H. Caceres, J.R. Griffiths, Acta Mater. 44 (1996) 25–33.
[28] G. Guiglionda, W.J. Poole, Mater. Sci. Eng. A319–321 (2001) 583–587.
[29] C. Xu, Z. Horita, T.G. Langdon, Acta Mater. 56 (2008) 5168–5176.
[30] M.J. Starink, A.-M. Zahra, Mater. Sci. Eng. A 241 (1998) 277–280.
[31] Y. Huang, J.D. Robson, P.B. Prangnell, Acta Mater. 58 (2010) 1643–1657.